Mechanical alloying in the Co-Fe-Ni powder mixture: Experimental study and molecular dynamics simulation

A.S. Rogachev, A. Fourmont, D.Yu. Kovalev, S.G. Vadchenko, N.A. Kochetov, N.F. Shkodich, Florence Baras, O. Politano

Mechanical alloying in the Co-Fe-Ni powder mixture: experimental study and molecular dynamics simulation.

A.S. Rogachev[1,*], A. Fourmont[2], D.Yu. Kovalev[1], S.G. Vadchenko[1], N.A. Kochetov[1], N.F. Shkodich[1], F. Baras[2], O. Politano[2]

[1]*Merzhanov Institute of Structural Macrokinetics and Materials Science, Russian Academy of Sciences, Chernogolovka, 142432 Russia*

[2]*ICB laboratory, UMR 6303 CNRS-Université Bourgogne Franche-Comté, 9 Av. Alain Savary, BP 47870, 21078 Dijon Cedex, France*

*Corresponding author: rogachev@ism.ac.ru

ABSTRACT

The formation dynamics of medium- entropy alloy CoFeNi has been studied both experimentally and theoretically in terms of molecular dynamic simulation. The results of experiments and modelling showed good qualitative agreement and supplemented each other. The synthesis was found to occur in two stages. (a) Refinement of crystallites and accumulation of structural defects take place due to severe plastic deformation and friction of metal particles that induce abnormally fast diffusive mixing of different metal atoms. This process results in formation of nanocrystalline intermediate alloy with a crystallite size of about 10 nm. (b) Recrystallization that leads to the nucleation and growth of multicomponent phase with a simple FCC crystal structure. A critical time for the onset of recrystallization depends on planetary milling regime and gaseous atmosphere in the milling jar.

Keywords: mechanical alloying, crystal structure, microstructure, molecular dynamics simulations, X-ray diffraction

1. Introduction

A ternary alloy CoFeNi was thoroughly studied during past 2-3 decades, mainly due to its very attractive magnetic properties. Soft ferromagnetic properties inhere in nanocrystalline [1] and amorphous [2] CoFeNi films, in spin valves and other multilayer structures that include thin layers of this alloy [3-5]. A very high magnetic saturation was reported for metastable CoFeNi films [6]. The electrodeposited thin films [1-6] and wires [7,8] of the CoFeNi alloy became prospective elements for various sensors, data storage and other electronic devices, as well as for spintronics applications [9].

After invention of high-entropy alloys (HEA) in the beginning of this century [10, 11], the ternary alloys CoFeNi, CoCrNi, etc. attract more attention as core systems of the 3d-transition metals family of HEAs. Chemical composition of these advanced materials can be

presented as CoCrFeNiX, where X = Al, Cu, Mn, or Ti [12–14]. Note that Co, Fe and Ni presents in all compositions, while adding fourth and fifth elements such as Al [15], Ti [16] or Cr [17] to this group bridges a gap between ternary principle elements alloys and high-entropy alloys that commonly include five or more components. In some cases, properties of ternary alloys were found to be better than properties of quinary alloys. For example, due to formation of nano-twinning net, the alloy CoCrFe possesses better mechanical properties at room and cryogenic temperature as compared to the HEA CoCrFeNiMn [18,19].

An emerging of new field of research and development requires novel methods for production of ternary alloys in the form of powders and bulk materials, in addition to electrodeposition technique previously used for obtaining thin CoFeNi soft magnetic films. Methods of arc melting [20] and additive manufacturing [21] were applied for obtaining bulk CoFeNi alloy and testing its mechanical properties. Mechanical alloying of the powders mixtures in vibratory mills allowed production of CoFeNi layers and nanolaminate structures on different substrates [22,23]. Recently, a vibratory mill was successfully applied for mechanical synthesis of ternary $Co_{40}Fe_{30}Ni_{30}$, $Co_{30}Fe_{40}Ni_{30}$ and $Co_{30}Fe_{30}Ni_{40}$ alloys after 7 h of the milling [24]. An effective method of high energy ball milling (HEBM) using planetary ball mills was applied to medium-entropy CoCrFeNi alloy [17] and several five-component HEAs [25-30] , however, mechanical alloying of the CoFeNi alloy has not been investigated up to now.

Experimental methods of studying dynamics of structure and phase transformations caused by HEBM are generally based on step-by step sampling of the powder blends, after different time of ball milling, and study these samples by means of SEM, TEM, XRD and other methods [29-31]. At the same time, the contemporary experimental methods don't allow *in situ* observation of atomic-scale transformations, induced by severe plastic deformation during HEBM. This problem can be partially solved using new methods of molecular dynamics simulations (MDS) applied to intense deformation of nanocrystalline powder blends [33,34].

In this work, we studied for the first time, experimentally and by MDS, dynamics of structure and phase transformations taking place during mechanical alloying of medium-entropy CoFeNi powder.

2. Materials and methods

Commercially available metal powders used as starting materials are listed in Table 1. It is worth noting that all three metal components have different crystal structures at normal conditions, but close atomic radii, which allows formation of solid solutions with simple atomic packings.

Table 1. Characteristics of powders used in experiments (all from Russian manufactures)

	Brand	Purity	Particle size, μm	Crystal structure	Atomic radius, Å [12]
Co	PK-1u	>99.35%	<71 μm	HCP	1.251
Fe	OChS	>99.9 %	10–20 μm	BCC	1.241
Ni	PNE-1	>99.5 %	~150 μm	FCC	1.246

The elemental metal powders were blended in equimolar proportions and placed in steel jars of a water-cooled planetary ball mills,10 g of powder mixture per a jar. Two types of high-energy mills were used in this work for synthesis of the same alloy. First, Activator-2S, had 2 jars with volume 250 cm^3 each, and was run at a rotating speed of 694 and 1388 rpm for the sun disk and grinding jars, respectively. The jars of Activator-2S were evacuated and then filled with Ar gas at 4 bar. Steel milling balls, 7 mm in diameter, were placed in the jar together with powder mixture. The second mill, AGO-2 (Novosibirsk, Russia), was rotated at 912 rpm, which corresponded to 2220 rpm for jars rotating speed. This mill also had 2 jars, 160 cm^3 each, that remained filled with atmospheric air at normal conditions, although all jars were hermetically closed during all period of mechanical alloying. The balls with diameter 9 mm was used in this planetary mill. For the both mills, ball-to-powder mass ratio was equal to 20 : 1 in all runs.

Simultaneous utilizing of two planetary mills helped us to reveal influence of HEBM condition, such as rotating speed and acceleration or gas atmosphere on dynamics of mechanical alloying.

The XRD analysis of powders was performed with a DRON-3M diffractometer (Russia). As a rule, Fe-K_α radiation ($\lambda = 0.19374$ nm) was used for the sake of better angular resolution. The SEM and EDS analyses were made using a LEO 1450 VP microscope (Carl Zeiss, Germany) equipped with an energy-dispersive X-ray spectrometer INCA 300. An average composition was detected by EDS analysis of the 16×12 μm area on the cross-section. In order to estimate homogeneity of microstructure and scattering of local compositions, numerous EDS analyses were made in random points on the surface of cross-section. In case of strong scattering, 16 points were tested for each sample; this number decreased to 5–6 points in case of uniform samples with minor fluctuations of local composition. Vickers microhardness (*H*v) was measured with a PMT3 tester (Russia) under a 50-g load. Local EDS analysis and microhardness measurements were made within alloy particles stacked at the surface of milling balls. The balls, together with the stacked layers of alloy particles, were cut using diamond saw, and their cross sections were mechanically polished for use in SEM, EDS, and *H*v studies.

Molecular dynamics simulations were performed using the LAMMPS software [35]. The atomic interactions were described by the Embedded Atom potential (EAM) proposed by Zhou et al. [36]. The equations of motion were integrated with a timestep of 1 fs. Periodic boundaries were applied in all three directions. The MDS procedure intends to mimic the HBEM process by performing cyclic plastic deformation of a simulation box containing several pure metallic grains. The initial polycrystalline structure with 18 grains of pure metals was created by using the Voronoi tessellation [37]. The average grain diameter was around 4 nm, and the initial dimensions of the simulation box was $9.3 \times 9.3 \times 9.3$ nm. The total energy of the system was first minimized at 0 K to allow local atomic rearrangement at the grain boundaries. Then, a 50 ps run in the NVT ensemble followed by a 50 ps run in the NPT ensemble permits to thermalize the system at 100 K (i.e. below room temperature to avoid thermally activated diffusion). Chemical

mixing started by applying 100 cyclical compressive deformation steps of 150 ps each. One cycle is made of 3 successive deformations along the *X*, *Y* and *Z* directions by rescaling the box each 0.1 ps. The final strain (e.g. in the compressed direction *X*) was 25% after 50 ps. The two other directions (*Y* and *Z*) can freely expand independently to ensure a zero pressure along these directions. After 50 ps, the same procedure was repeated for the two other directions to complete a full cycle [38]. The virtual process simulates the plastic deformation of metallic particles during HEBM. This procedure is later mentioned as PDM (Plastic Deformation Mixing).

Results of MDS were analyzed with the OVITO visualization software [39]. The adaptive common neighbor analysis (a-CNA) permitted to identify the local atomic configuration. The well-defined peaks in the Radial Distribution Function gave the evaluation of lattice parameters. The MicroChemical Inhomogeneity (MCI) introduced by Li *et al*. [40] was adapted to provide a measure of the local chemical mixing for a given atom (for a detailed description see [33]).

3. Experimental results

Three metals of the iron group, Co, Fe, and Ni, constitute a ternary core of HEAs of the 3*d* transition metals family. These metals have close atomic radii, but different crystal structures (Table 1). During the HEBM process, all atoms intermix and form a uniform alloy. Dynamics of the crystal structure transformations in the Co + Fe + Ni mixture is shown in Fig. 1 for two different planetary mills. An XRD pattern of initial mixture demonstrates superposition of diffraction peaks of the individual metals (Fig. 1a). Due to close atomic sizes, intense peaks of the Co (002), Fe (110), and Ni (111) partially overlap, because they have very close angular positions (2θ): 57.175, 57.058, and 56.837, respectively (Fig. 1b). After 5 min of HEBM, all these 3 peaks fused together forming one broad peak. This peak gradually becomes even broader, and its maximum slowly drifts toward smaller angles during subsequent 25 min in case of Activator-2S or only 10 min in case of AGO-2 (Fig. 1). After 20 min of HEBM in AGO-2, or 60 min in Activator-2S, the width of this peak suddenly decreases, and its maximum jumps left

over the 2θ interval of 0.5–0.6 deg (in Figs. 1b, d, the peak jump marked with the arrow). This transformation indicates the formation of multicomponent FCC phase (Figs. 1a, c). Further milling does not change notably the XRD pattern of the alloy.

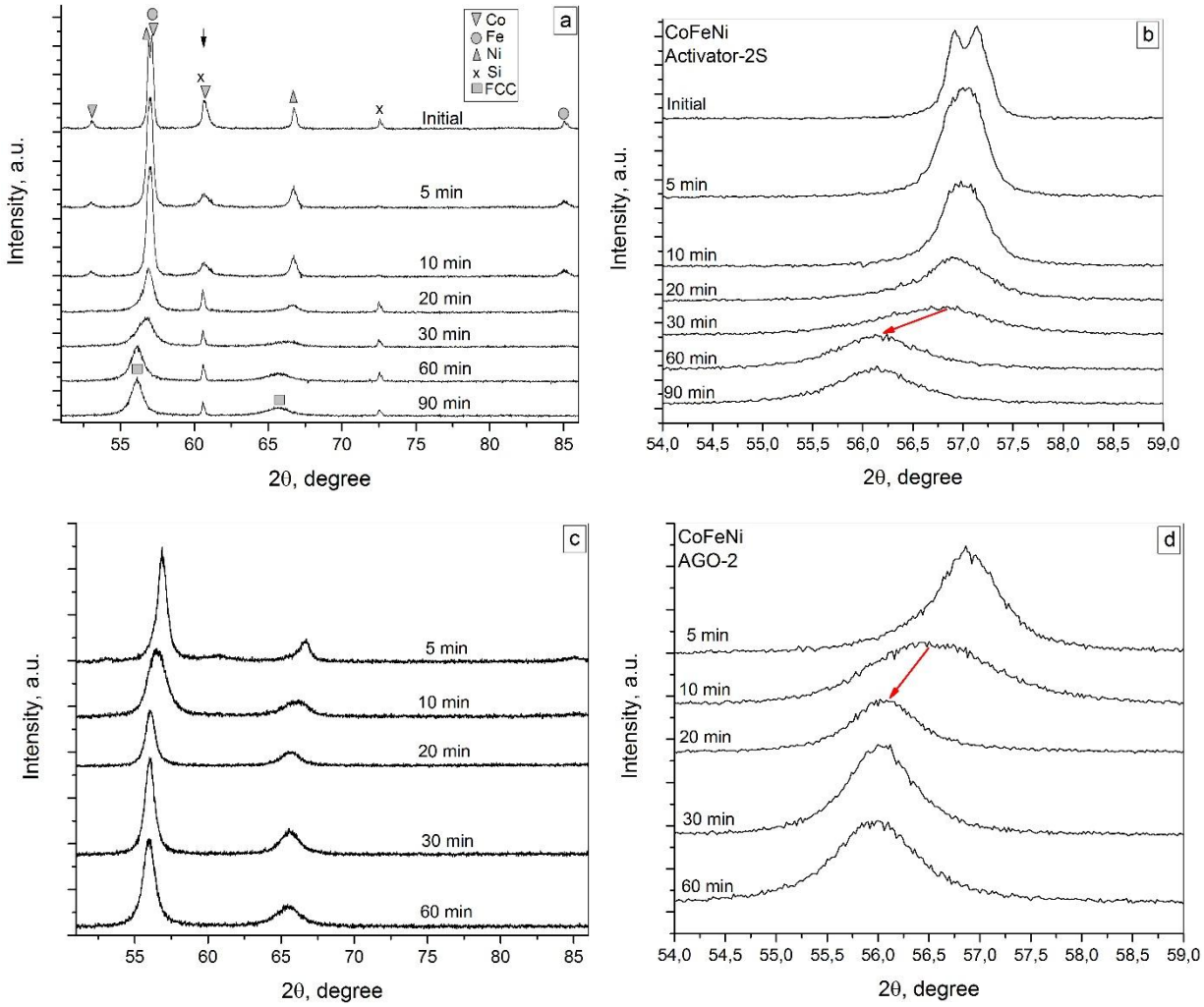

Figure 1. XRD patterns of the Co–Fe–Ni system activated in Activator-2S (a, b) and AGO-2 (c, d): overall view (a, c) and the expanded 100% peak (b, d).

Interplanar distances calculated basing on the position of major (100%) peak, presented in Fig. 2, show expansion of crystal lattice by approximately 1.5%. Dynamics of this transformation differs for Activator-2S and AGO-2 mills.

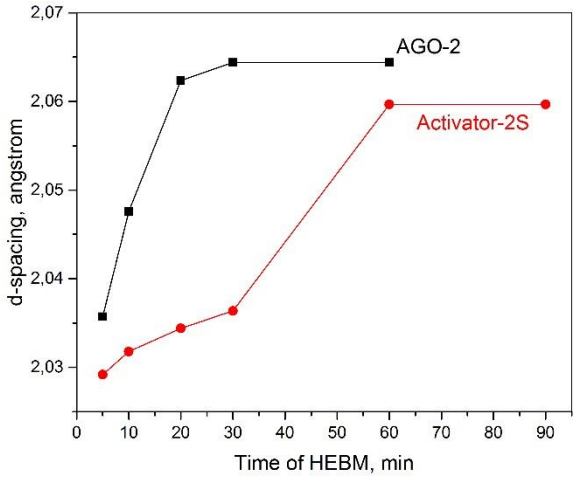

Figure 2. (Color online) Evolution of interplanar distance (*d*-spacing) in the course of HEBM as evaluated from position of the strongest XRD peak.

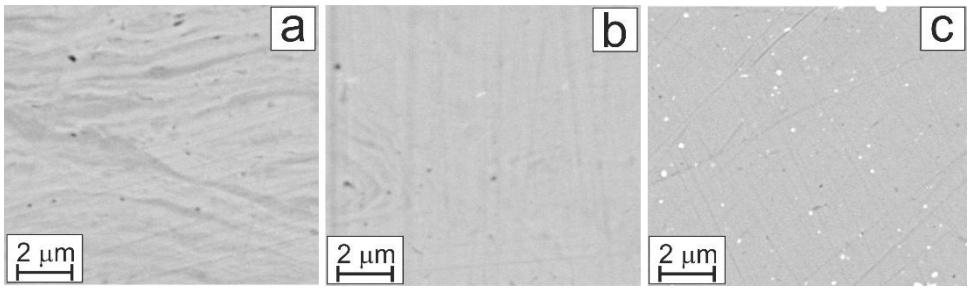

Figure 3. SEM image of the Co–Fe–Ni alloy after different time of HEBM (AGO-2): 5 (a), 10 (b), and 30 min (c); white spots corresponds to contaminations with Wood's alloy used in the preparation of cross-section.

Cross-sections of the powder particles formed during HEBM (Fig. 3) reveal that the inhomogeneity of chemical composition that remained after 5 min of milling (Fig. 3a), diminish after 10 min of milling (Fig. 3b) and disappeared in 30 min of mechanical processing (Fig. 3c).

Results of local EDS analysis for different randomly selected points of sample cross-section are presented in the form of ternary diagram in Fig. 4a. Significant scattering of data points is observed after 5-min HEBM because some local regions (spots) contained more Fe,

others more Co, and some more Ni. Also, some spots have a composition close to pure Fe or pure Co. With increasing duration of HEBM, all points gather together in the middle of the diagram in the vicinity of concentrations 33/33/33 (at.%). After 5 min of HEBM, the concentrations of Co and Fe dispersed from 0 to 100 at. % while the concentration of Ni – from 0 to 60 at. % (Figs. 4b, c, d). After 10 min, the range of data scattering gets narrower, and all three metal concentrations practically converge after 20 min of HEBM. Based on these results, we may suppose that a 3-component matrix phase with relatively uniform concentration of all metals was formed after 20-min HEBM (AGO-2). This is in good agreement with the transformation of crystal structure (Figs. 1c, d). It is worth noting that this transformation occurs faster in AGO-2 (air atmosphere, 912/2220 rpm) as compared to Activator-2S (Ar atmosphere, 694/1388 rpm).

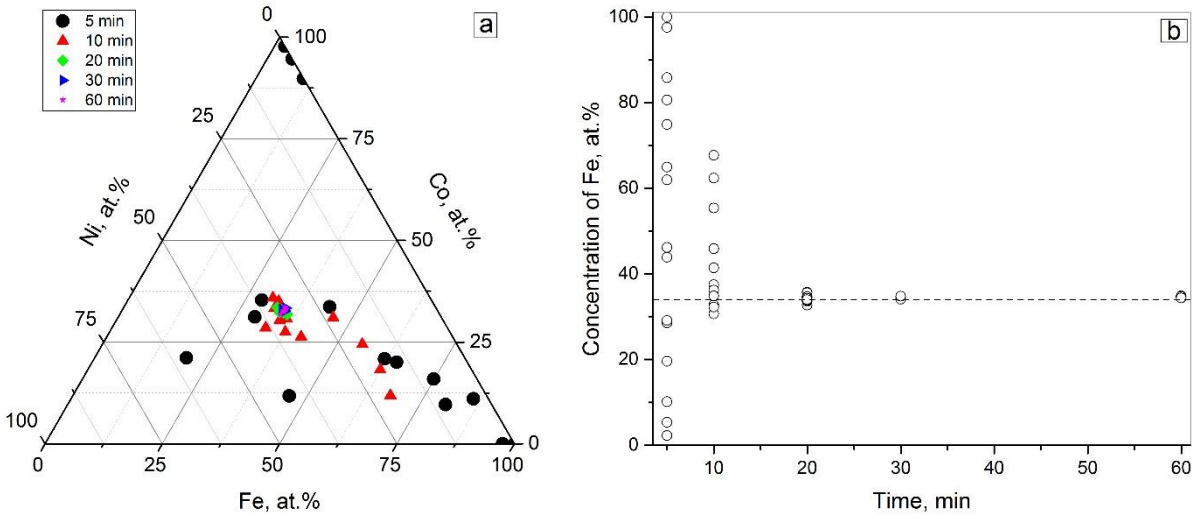

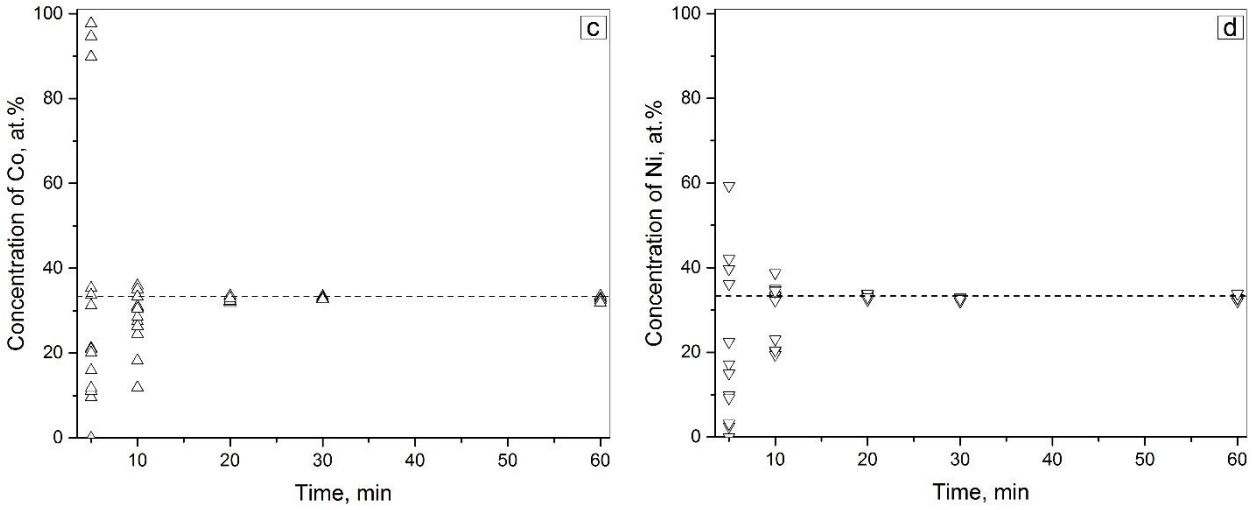

Figure 4. (Color online) Results of local EDS analysis taken in random points of the cross-sections of powder particles, presented as ternary diagram (a) and as concentration of individual components (b-d). AGO-2 mill.

Basing on the experimental results, we can outline some common features of phase and structural transformations that take place during mechanical alloying of 3*d* transition metals. Multiple severe plastic deformations of ductile metals, cold welding, and mutual interdiffusion during HEBM cause a decrease in crystallite size and an increase in concentration of lattice defects and grain boundaries, which result in broadening XRD peaks. When structural distortions achieve some critical level, a new phase of multicomponent alloy starts to form, and all intermediate solid solutions formed by Fe, Ni, and Co crystal structures convert into this phase.

Microhardness of the alloy particles slightly increases during the first 20 min of HEBM and then levels-off (Fig. 5). Large spread in *H*v values indicates that the extent of local cold-working markedly changes across the alloy particles.

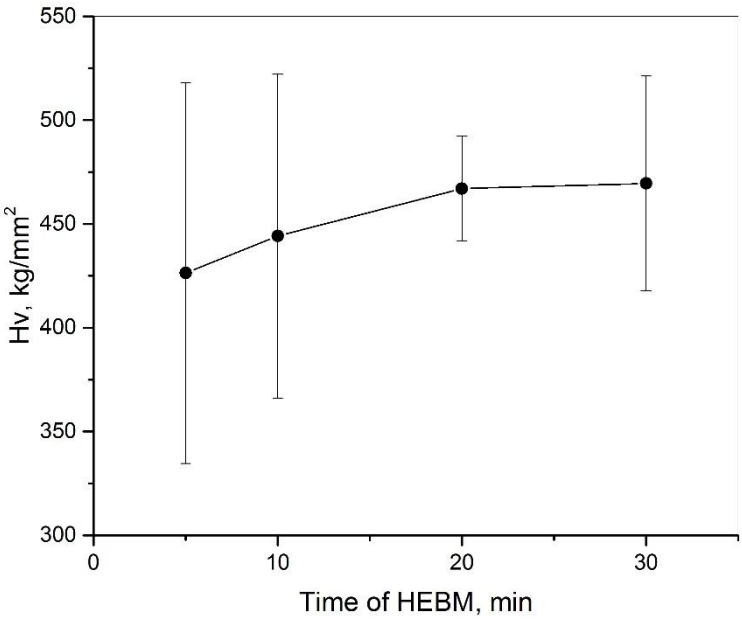

Figure 5. Microhardness *H*v for CoFeNi powders as a function of HEBM time (AGO-2).

4. Molecular Dynamics Simulation

A simulation box created for the MDS study of mechanical alloying (Fig. 6) was composed of 18 pure metal grains: 6 grains of Co with HCP structure, 6 grains of Fe with BCC structure, and 6 grains of Ni with FCC structure. Atoms located in grains boundaries could not be attributed to the FCC, BCC or HCP structures and considered as the amorphous phase. The grains had irregular shape; every grain contained from 3107 to 4831 atoms. A typical size of the grain can be estimated as 4 nm (in diameter, if we approximate the grain by spheres) but can reach as much as 5–6 nm (by computing the maximal grain width). As compared to 'real experiments', the time and length scales reachable by MDS may appear limited. However, MDS permits to have an '*in-situ*' visualization of the atomic processes occurring during ball milling and, therefore, to reveal some important features of the mechanical alloying mechanism.

An intense mixing of the metal atoms began from the first cycles of deformation and completed after 100 cycles (Fig. 7). All 3 types of the crystal structures persisted after 250 cycles of deformation. Atomic fraction of the different types of crystal structures show notable

fluctuations due to the limited size of simulation box. At the same time, the average content of BCC, FCC, HCP and amorphous structures remains approximately stationary during 250 cycles of deformation (Fig. 7 and Fig. 8). The system remained partly crystallized over deformation. We noted fluctuations in FCC and BCC structures around 30 at. % each. A fifth of atoms were in the amorphous state. These atoms were initially located at the interface between metallic particles. At the end of the cyclic deformation, these amorphous atoms are present inside crystallized regions and generally surround points defects, voids or indicate highly deformed zones. A tenth of atoms are HCP; in the beginning these atoms corresponds to pure Co. After deformation, HCP atoms indicate linear defects in FCC crystallized regions (i.e. twins and stacking faults). Thus, the cyclic deformation leads to a dual HEA phase (BCC/FCC) with a homogenous distribution of 3 constitutive elements. This MDS result looks inconsistently in comparison with experimental data (see Fig. 1) that show conversion of all initial phases into a single FCC phase. This discrepancy is likely due to the potential used in this work. Indeed, 250 ideal equimolar CoFeNi BCC and FCC structures were generated following the Random Substitution Mixing (RSM) procedure described in [33]. For both structures, the average cohesive energy computed is identical and equal to –4.358 eV. As a consequence, the Zhou's potential is unable to discriminate the relative stability between FCC and BCC phases.

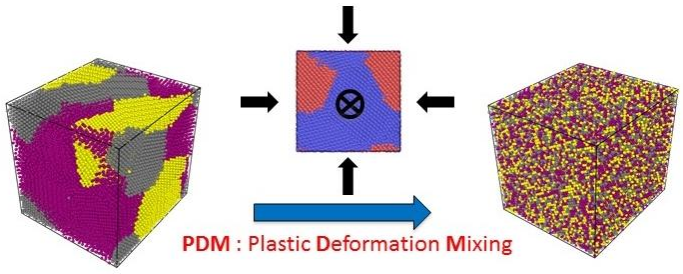

Figure 6. (Color online) Schematic of the molecular dynamic simulation of mechanical alloying. See also supplementary video file S1.

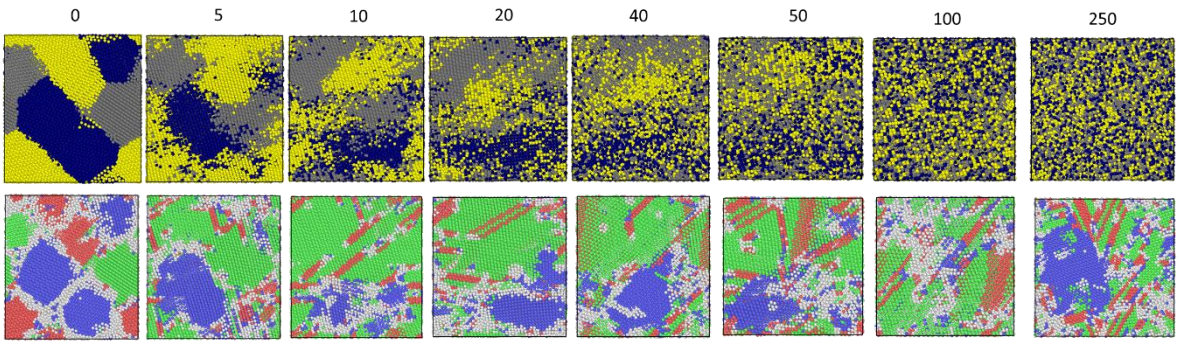

Figure 7. (Color online) Snapshots of a slice of 2 nm during the plastic deformation mixing as dependent on the number of deformation cycles (from 0 to 250). Top line corresponds to chemical identity: yellow corresponds to Co atoms (light gray in grayscale image), gray to Ni, blue to Fe (dark gray in grayscale image); bottom line corresponds to structural identity: blue (dark gray) corresponds to BCC structures, red (middle dark gray) to HCP, green (middle gray) to FCC, light gray to amorphous or unidentified ones. Number of deformation cycles are shown at the top of the figure.

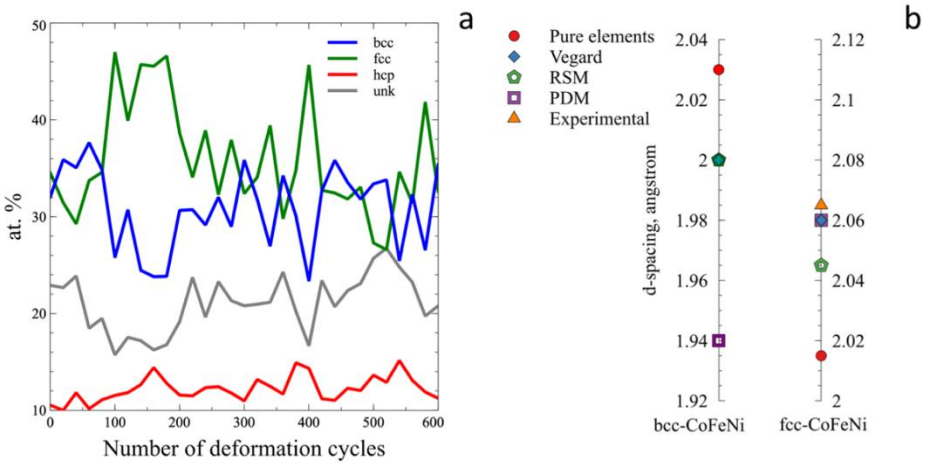

Figure 8. (Color online) (a) Crystalline structure percentage as a function of deformation cycles. (b) Interplanar distance (*d*-spacing) corresponding to the (111) FCC plan and (110) BCC plan calculated with different techniques: Vegard rule, Random Substitution Mixing (RSM), and Plastic Deformation Mixing (PDM).

The radial distribution function was computed for FCC and BCC atoms, before and after 250 deformation cycles (Fig. 9a). We noted that the first peak is at the same position for both FCC and BCC atoms, prior and after deformation. In the initial system, the superposition of the first peaks is actually due to the particular relation

$$\sqrt{1/2}\, a_0(\mathrm{Ni}) = 2.4887 \approx \sqrt{3/4}\, a_0(\mathrm{Fe}) = 2.4819.$$

It appears that the deformation does not alter the location of the first peak. In other words, the first shell of atoms remains at the same distance for both structures. We noted a broadening of the second peaks with a significant shift for BCC-atoms to lower values and a slight shift to larger(higher) values for FCC-atoms. The second BCC-shell became very close to the first shell. For the FCC structure, RSM, PDM and Vegard's estimations are very close to each other (see Fig. 8b). The distribution of potential energy/atom prior deformation for each constituent is presented in Fig. 9b. Only atoms in the reference crystallographic structure were selected (HCP-Co, BCC-Fe, and FCC-Ni). We observed a slight shift to lower values in comparison with the cohesive energy of pure elements and broadening of the distributions that may be attributed to the small grain size in the initial system. After deformation, the distribution peaks are shifted to higher values for FCC-Co and FCC-Fe as compared to the value of pure elements. Nickel atoms keep the same potential energy prior and after deformation. This reflects the microscopic rearrangement associated with the formation of the solid solution.

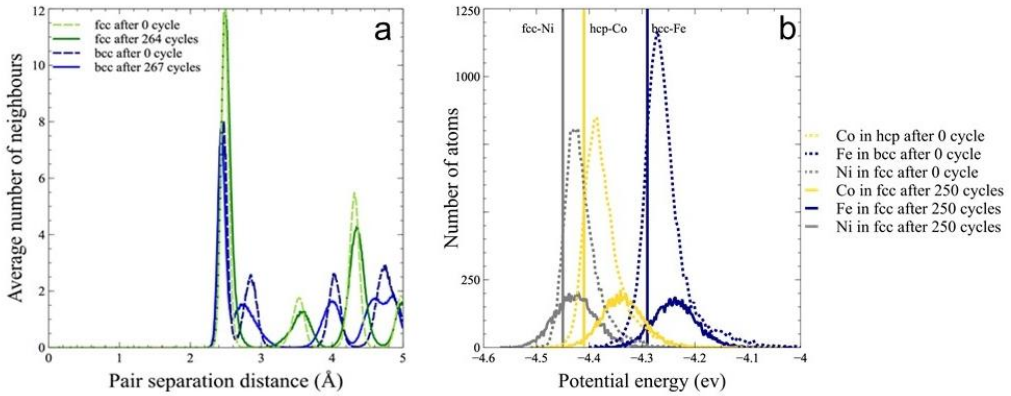

Figure 9. (Color online) (a) Coordination analysis of the equimolar Co Fe Ni system before and after 264 and 267 deformation cycles. (b) Histogram of potential energy per atom for selected groups of atoms before and after 250 deformation cycles.

Figure 10 depicts the microscopic configuration in different (111)-planes of the FCC solid solution and the corresponding mixing order parameter. We measured the composition of the solid solution that is equimolar. This is reflected at the atomic level by a random distribution of the three types of atoms. Some atoms of the same species may form a cluster in a given plane but the cluster disappears in adjacent planes. The mixing order parameter measured by the MicroChemical Inhomogeneity per atom (MCI/atom) is evaluated in 3D. We noted that MCI fluctuates around zero. This result indicates an effective mixing between chemical species in the solid solution. The same observations hold in the case of (101) planes of the BCC solid solution. Because of the relationship (1), there exists an epitaxy between (111)-FCC and (110)-BCC planes that facilitates the transition between the two structures over deformation.

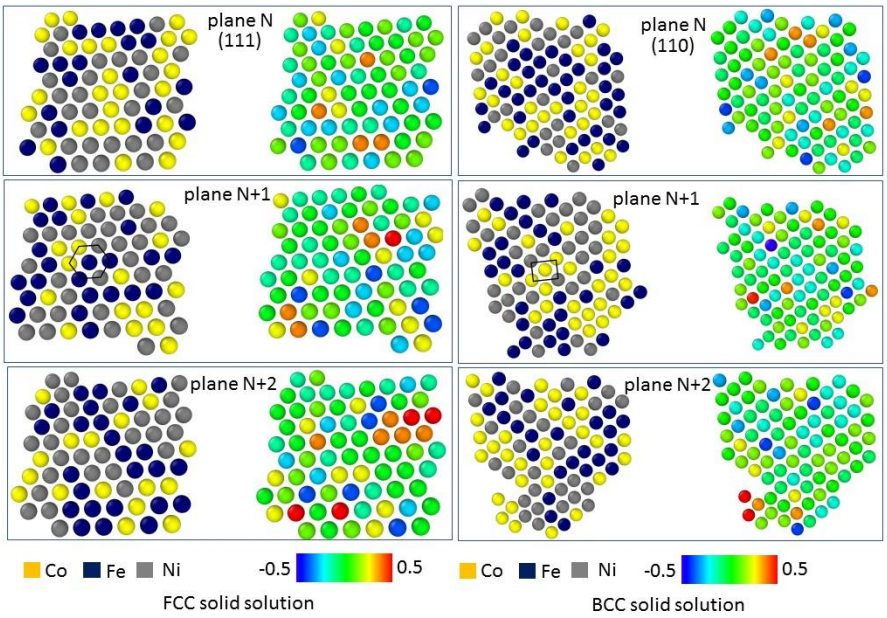

Figure 10. (Color online) Snapshots of three successive (111) planes in FCC and (110) BCC Co–Fe–Ni solid solution: chemical configuration (left) and MicroChemical Inhomogeneity (MCI)/atom (right).

5. Discussion

As compared to experiments, molecular dynamics simulations mimic the last steps of the mechanical alloying. Indeed, the simulated crystallites are already nanometric and a high concentration of lattice defects appears during the first deformation cycles. Hence, the critical level of structural distortions is rapidly achieved. Nevertheless, in spite of difference in spatial and temporal scales between experiments and MDS, comparison of these results can shed light on the mechanism of mechanical synthesis of the ternary alloy. Actually, MDS allow us to visualize the formation of the multicomponent alloy at the atomic level. Let us consider cross-section of the initial MDS-cube and mark boundaries between elemental crystallites with white lines (Fig. 11a). The snapshots made after definite cycles of deformation (Figs. 11b–f) show intense migration and destruction of the inter-crystalline boundaries and atomic mixing that occurs rapidly for all elements. A ballistic diffusion coefficient [41] has been roughly estimated as 10^{-9} m^2/s. This value is comparable with typical diffusion coefficient in molten metals and

much higher than diffusivity in solids at moderate temperature. For example, diffusion coefficient of Fe atoms in solid Ni is about 10^{-16}–10^{-15} m^2/s at 1200 K, diminishing down to zero at room temperature. The results of experimental study (cf. Fig. 1 and Fig. 2) show that homogenization of the chemical composition and formation of the single FCC phase occur between 10 min and 20 min of HEBM. Initial size of the Ni powder particles is about 150 μm, diffusion path for the Fe atoms should be about half of this size. If atomic diffusion were the only mechanism for alloying, a required diffusion coefficient evaluated by formula $D = L^2/t$, where the diffusion path $L \approx 75$ μm, the HEBM time $t \approx 600$–1200 s would be not less than 10^{-12}–10^{-11} m^2/s. Thus, the diffusivities of metals calculated in the frame of MDS and estimated experimentally are much higher than diffusion coefficients of the considered metal atoms in bulk solids. Two factors, both related to severe plastic deformation of metals, can cause the sharp decreasing of the time interval required for atomic intermixing. First, deformation of the initial metal particles results in the formation of thin layers, which decreases diffusion path L down to a few micrometers or less. Second, diffusivity can be significantly increased due to abnormally high concentration of vacancies and other crystal lattice defects generated by intense plastic deformation [42, 43]. Qualitative mechanism of mechanically stimulated atomic mixing during HEBM was suggested for the Ni–Al system [31]. It is based on assumption that plastic flow of ductile metal (e.g. Al) along the interphase boundary carries away single atoms and atomic clusters of other metal (e.g. Ni). Anyway, atomic mixing occurs anomalously fast under the action of high-energy ball milling.

In addition, although Fe is BCC and is likely the hardest to dissolve, it seems to take part in the solid solutions formation at the same rate as the others. In spite of the discrepancy concerning the relative stability of ternary FCC and BCC phases with the Zhou's potential, it is interesting to note that most of the systems remain crystalline during the formation of solid solutions.

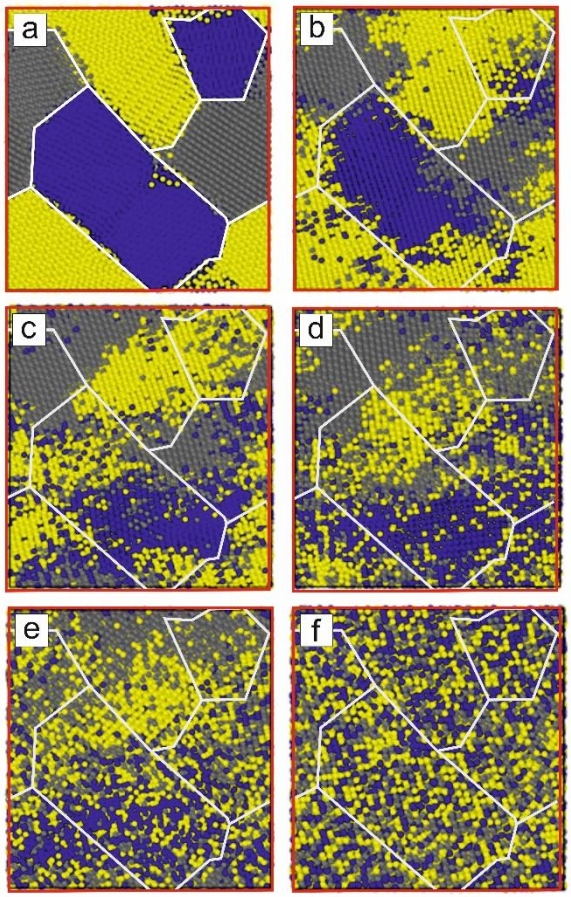

Figure 11. Dynamics of atomic mixing during cyclic deformation: (a) initial structure before deformation, and after 5 (b), 10 (c), 20 (d) 40 (e), and 100 deformation cycles (f).

Broadening of XRD peaks in course of HEBM (Fig. 1) indicates decreasing of crystalline size and accumulation of micro-stresses and lattice distortions. Estimation of crystalline size (*d*) by Scherrer formula shown that *d* decreased down to 8.2-9.0 nm before the XRD peaks "jumps", and sharply increased up to 12.9-15.7 nm after the jump. It must be underscored that the Scherrer method does not consider fine effects (such as microstress, hardware broadening or concentrations of dislocations), therefore, these values are quite rough approximation. Nevertheless, the effect of sudden peak shifting and narrowing occurring after some critical time of HEBM is so evident, that we cannot ignore it. When the single FCC phase forms, the width of the XRD peak decreases simultaneously with the drift of its position, thus indicating a growth in

crystallite size. We can surmise that crystalline grains of the FCC phase nucleate and grow in a very fine-grained polycrystalline matrix formed due to multiple severe plastic deformation of individual metal crystallites. Thus, the process of mechanical synthesis of medium-entropy alloy CoFeNi by HEBM consists of two stages. (a) Due to very intense plastic deformation, the crystalline sizes of initial metals diminish down to several nanometers, and the abnormally fast diffusion promotes the intermixing of components on an atomic scale. As a result, intermediate nanocrystalline alloy forms with a high concentration of intergrain, interphase and intercrystallite boundaries, crystal lattice defects, and chemical inhomogeneities. Such alloy should possess some excess of free energy and likely be metastable. (b) When the amount of the excess energy achieves some critical value (e.g. when crystallite size decreases down to ~10 nm), relatively fast recrystallization with phase transformation happens, which results in the formation of single multicomponent phase.

A comparison of the obtained results with other works shed some light on intrinsic mechanisms of mechanical alloying. First of all, very short time of the final FCC phase formation in our experiments must be explained. As it was stated in the previous works, multicomponent solid solutions form after 15-40 h of high-energy ball milling [44]. The ternary Co-Fe-Ni alloys were obtained after 7 h in shaking mill [24]. In our case, single-phase and chemically uniform alloy forms between 10 and 20 min of HEBM in AGO-2 (Fig. 1c,d; Fig. 3; Fig. 4), or between 30 and 60 min in Activator-2S (Fig. 1a,b) mills. The results of MDS show that complete mixing of the components at atomic scale occurs after 50 – 100 cycles of deformation (Fig. 7; Fig. 11). This effect, most likely, is due to higher intensity of deformation and absence of liquid process control agent in our experimental work and modelling. Commonly, air-cooled planetary ball mills with rotating speed 300-350 rpm or vibratory mills are used for synthesis. Using high-intensity water cools mills (Activator-2S and AGO-2) with rotating speed 694 – 912 rpm in this work provides higher degree of plastic deformation of the initial metals, which sharply accelerates alloy formation process. Using of different milling equipment and,

therefore, different energies of the milling balls impacts and friction, results in quite different time that is required for alloying. The MDS results confirm that if degree of deformation reaches 25%, just a few tens of deformation cycles become enough to mix all atoms at atomic scale. Therefore, intensity of severe plastic deformation plays a key role for intensification of interdiffusion processes and multicompoment alloy formation. Other factors are properties of the boundaries between components. Evidently, clean boundary between phases should promote cold welding and jumps of atoms across the boundary from one phase to another. This process can be retarded if any liquid process control agent (toluene, heptane, ethanol, etc.), that is often used in HEBM, penetrates along boundaries between phases. Our results show that dry mixing allows obtaining single phase alloy in a very short time.

Three types of the interphase boundaries exist in the initial system, which are Co-Fe, Co-Ni, and Fe-Ni. Consequently, we may expect formation of six binary solid solutions at early stage of mixing: Co(Fe), Co(Ni), Fe(Co), Fe(Ni), Ni(Co), and Ni(Fe). Depending on the base matrix element, these phases should have different crystal structures, FCC, BCC or HCP (see Table 1). As it was shown by Vaidya et al. [45], crystal structure of the starting binary phase influences phase constitutions of final multicomponent alloy AlCoCrFeNi produced after 30 – 70 h of mechanical alloying. In our case, however, uniform FCC structure formed after 20 – 60 min of HEBM due to very intense plastic deformation, dry friction of the components and simpler composition of the final alloy. Distribution of local chemical compositions at early stages, after 5 and 10 min of HEBM (Fig. 4,a), allow us to surmise that primary solid solutions were formed mostly on the base of Fe, because experimental points locate along line connecting middle point of equiatomic composition CoFeNi with Fe-corner of the diagram.

6. Conclusions

We have studied experimentally and theoretically, using high-energy ball milling and molecular dynamic simulation, the dynamics and mechanism of mechanical synthesis of

medium-entropy alloy CoFeNi. Results of both experimental and modelling approaches are in a good qualitative agreement, supplement each other, and allow the following conclusions.

- ✓ The mechanical synthesis of multicomponent alloy occurs in two stages.
- ✓ At the first stage, refinement of crystallites and accumulation of crystal structure defects take place due to severe plastic deformation and friction of metal particles that induce abnormally fast diffusive intermixing of different metallic atoms. This process results in formation of nanocrystalline intermedium alloy with a crystallite size of about 10 nm.
- ✓ At the second stage, recrystallization occurs, which leads to the nucleation and growth of multicomponent phase(s) with a simple FCC.
- ✓ A critical time for the onset of recrystallization depends on planetary milling regime and gas atmosphere in the milling jar. Shorter time is required for the formation of uniform multicomponent phase, if the HEBM is carried out with air atmosphere inside the milling jar, in comparison with the inert gas (Ar) atmosphere. Increasing rotating speed of the mill also decreases this time.
- ✓ Optimization of milling regimes allows producing single-phase CoFeNi alloy after 30-60 min of planetary ball milling.

Acknowledgements

We are grateful to Dr. Yu. Scheck for fruitful discussions, Mrs. N. Mukhina for SEM/EDS measurement, and Mrs. A. Belikova for H_v measurements.

Funding

This work was supported by Russian Foundation for Basic Research (project no. 18-53-15006) in the framework of the International French–Russian PRC CNRS-RFBR project SHEA.

References

1. E.H. du Marchie van Voorthuysen, F.T. ten Broek, N.G. Chechenin, D.O. Boerma, Thermal stability of the in-plane magnetic anisotropy and the coercivity of nanocrystalline CoFeNi films. Journal of Magnetism and Magnetic Materials 266 (2003) 251–257. doi:10.1016/S0304-8853(03)00141-0
2. A. Kaufler, Y. Luo, K. Samwer, Magnetic properties and thermal stability of CoFeNi-based amorphous films. J. Mater. Sci. 39 (2004) 3941 – 3947.
3. Hideaki Fukuzawa, Hitoshi Iwasaki, Katsuhiko Koi, Masashi Sahashi, Soft magnetic characteristics of an ultrathin CoFeNi free layer in spin-valve films. Journal of Magnetism and Magnetic Materials 298 (2006) 65–71. doi:10.1016/j.jmmm.2005.03.010
4. S. Kalsen, M. Alper, H. Kockar, M. Haciismailoglu, O. Karaagac, H. Kuru, Properties of electrodeposited CoFeNi/Cu superlattices: The effect of CoFeNi and Cu layers thicknesses. J. Supercond. Nov. Magn. 26 (2013) 813–817. DOI 10.1007/s10948-012-1912-7
5. M.A. Milyaev, N.S. Bannikova, L.I. Naumova, V.V. Proglyado, E.I. Patrakov, I.Yu. Kamenskii, V.V. Ustinov, Magnetoresistance of CoFeNi/Cu superlattices differing in the ferromagnetic alloy composition. Physics of Metals and Metallography, 120 (2019) 831–837. DOI: 10.1134/S0031918X19090084
6. I. Tabakovic, V. Venkatasamy, Preparation of metastable CoFeNi alloys with ultra-high magnetic saturation (Bs = 2.4–2.59 T) by reverse pulse electrodeposition. Journal of Magnetism and Magnetic Materials 452 (2018) 306–314. https://doi.org/10.1016/j.jmmm.2017.12.003
7. H. García-Miquel, G.V. Kurlyandskaya, Low ¯eld microwave absorption and magnetization process in CoFeNi electroplated wires. Chinese Physics B 17(4) (2008) 1430-06.

8. H. García-Miquel, V.M. García-Chocano, G.V. Kurlyandskaya, Circular Magnetization Processes In CoFeNi Electroplated Wires. Solid State Phenomena 152-153 (2009) 341-344. doi:10.4028/www.scientific.net/SSP.152-153.341
9. M.A. Milyaev, N.S. Bannikova, L.I. Naumova, V.V. Proglyado, E.I. Patrakov, N.P. Glazunov, V.V. Ustinov, Effective Co-rich ternary CoFeNi alloys for spintronics application. Journal of Alloys and Compounds 854 (2021) 157171. https://doi.org/10.1016/j.jallcom.2020.157171
10. J.-W. Yeh, S.-K. Chen, S.J. Lin, J.-Y. Gan, T.-S. Chin, T.-T. Shun, C.-H. Tsau, S.-Y. Chang, Nanostructured high-entropy alloys with multiple principal elements: Novel design concepts and outcomes, Adv. Eng. Mater. 6 (2004) 299-303.https://doi.org/10.1002/adem.200300567.
11. B. Cantor, I.T.H. Chang, P. Knight, A.J.B. Vincent, Microstructural development in equiatomic multicomponent alloys, Mater. Sci. Eng. A 375–377 (2004) 213–218. https://doi.org/10.1016/j.msea.2003.10.257.
12. D.B. Miracle, O.N. Senkov, A critical review of high entropy alloys and related concepts, Acta Mater. 122 (2017) 448–511. https://doi.org/10.1016/j.actamat.2016.08.081.
13. B.S. Murty, J.W. Yeh, S. Ranganathan, P.P. Bhattacharjee, High-Entropy Alloys, Amsterdam, Elsevier, 2019.
14. A.S. Rogachev, Structure, stability, and properties of high-entropy alloys, Phys. Met. Metallogr. 121(8) (2020) 733–764. doi: 10.1134/S0031918X20080098.
15. T.T.Zuo, R.B.Li, X.J.Ren, Y.Zhang, Effects of Al and Si addition on the structure and properties of CoFeNi equal atomic ratio alloy. Journal of Magnetism and Magnetic Materials 371 (2014) 60–68. http://dx.doi.org/10.1016/j.jmmm.2014.07.023
16. S. Romankov, Y.C. Park, I.V. Shchetinin, Structural transformations in (CoFeNi)/Ti nanocomposite systems during prolonged heating. Journal of Alloys and Compounds 745 (2018) 44-54. https://doi.org/10.1016/j.jallcom.2018.02.150

17. Jie Xu, Xuan Kong, Minghui Chen, Qunchang Wang, Fuhui Wang, High-entropy FeNiCoCr alloys with improved mechanical and tribological properties by tailoring composition and controlling oxidation. Journal of Materials Science & Technology 82 (2021) 207–213. https://doi.org/10.1016/j.jmst.2020.12.042
18. Zhang Z., Sheng H., Wang Z., Gludovatz B., Zhang Z., George E.P., Yu Q., Mao S.X., Ritchie R.O. Dislocation mechanisms and 3D twin architectures generate exceptional strength-ductility-toughness combination in CrCoNi medium-entropy alloy // Nature Communications. V. 8. Art. 14390. P. 1-8.
19. Laplanche G., Kostka A., Reinhart C., Hunfeld J., Eggeler G., George E.P. Reasons for the superior mechanical properties of medium-entropy CrCoNi compared to high-entropy CrMnFeCoNi // Acta Mater. 2017. V. 128. P. 292-303.
20. Zhijun Wang, Sheng Guo, Qing Wang, Zhiyuan Liu, Jincheng Wang, Yong Yang, C.T. Liu, Nanoindentation characterized initial creep behavior of a high-entropy-based alloy CoFeNi. Intermetallics 53 (2014) 183-186. http://dx.doi.org/10.1016/j.intermet.2014.05.007
21. M.S.K.K.Y. Nartu, A. Jagetia, V. Chaudhary, S.A. Mantri, E. Ivanov, N.B. Dahotre, R.V. Ramanujan, R. Banerjee, Magnetic and mechanical properties of an additively manufactured equiatomic CoFeNi complex concentrated alloy. Scripta Materialia 187 (2020) 30–36. https://doi.org/10.1016/j.scriptamat.2020.05.063
22. S. Romankov, Y.C. Park, I.V. Shchetinin, Mechanical intermixing of elements and self-organization of (FeNi) and (CoFeNi) nanostructured composite layers on a Ti sheet under ball collisions. Journal of Alloys and Compounds 653 (2015) 175-186. http://dx.doi.org/10.1016/j.jallcom.2015.08.269
23. S. Romankov, Y.C. Park, I.V. Shchetinin, Deformation-induced plastic flow and mechanical intermixing of intentionally introduced impurities into a Ni sheet under ball

collisions. Journal of Alloys and Compounds 694 (2017) 1121-1132. http://dx.doi.org/10.1016/j.jallcom.2016.10.137

24. L.G. Betancourt-Cantera, F. Sánchez-De Jesús, A.M. Bolarin-Miró, A. Gallegos-Melgar, Jan Mayen, J.A. Betancourt-Cantera, Structural analysis and magnetic characterization of ternary alloys (Co-Fe-Ni) synthesized by mechanical alloying. Journal of Materials Research and Technology 9(6) (2020) 14969-14978. https://doi.org/10.1016/j.jmrt.2020.10.068
25. K.B. Zhang, Z.Y. Fu, J.Y. Zhang, J. Shi, W.M. Wang, H. Wang, Y.C. Wang, Q.J. Zhang, Nanocrystalline CoCrFeNiCuAl high-entropy solid solution synthesized by mechanical alloying, J. Alloys Comp. 485 (2009) L31–L34. doi:10.1016/j.jallcom.2009.05.144.
26. W.P. Chen, Z.Q. Fu, S.C. Fang, H.Q. Xiao, D.Z. Zhu, Alloying behavior, microstructure and mechanical properties in a FeNiCrCo0.3Al0.7 high entropy alloy, Mater. Des. 51 (2013) 854–860. https://doi.org/10.1016/j.matdes.2013.04.061.
27. W. Ji, W. Wang, H. Wang, J. Zhang, Y. Wang, F. Zhang, Z. Fu, Alloying behavior and novel properties of CoCrFeNiMn high-entropy alloy fabricated by mechanical alloying and spark plasma sintering, Intermetallics 56 (2015) 24–27. http://dx.doi.org/10.1016/j.intermet.2014.08.008.
28. F.Prusa, A. Senkova, V. Kucera, J. Capek, D. Vojtech, Properties of high-strength ultrafine-grained CoCrFeNiMn high-entropy alloy prepared by short-term mechanical alloying and spark plasma sintering. Mater. Sci. Eng. A. 734 (2018) 341–352. https://doi.org/10.1016/j.msea.2018.08.014.
29. S.G. Vadchenko, A.S. Rogachev, D.Yu. Kovalev, I.D. Kovalev, N.I. Mukhina, TiZrNiCuAl and TiNbNiCuAl alloys by thermal explosion and high-energy ball milling, Int. J. Self-Propag. High-Temp. Synth. 28 (2019) 137–142. doi: 10.3103/S1061386219020122.

30. A.S. Rogachev, S.G. Vadchenko, N.A. Kochetov, S. Rouvimov, D.Yu. Kovalev, A.S. Shchukin, D.O. Moskovskikh, A.A. Nepapushev, A.S. Mukasyan, Structure and properties of equiatomic CoCrFeNiMn alloy fabricated by high-energy ball milling and spark plasma sintering, J. Alloys Comp. 805 (2019) 1237–1245. https://doi.org/10.1016/j.jallcom.2019.07.195.
31. A.S. Rogachev, N.F. Shkodich, S.G. Vadchenko, F. Baras, D.Yu. Kovalev, S. Rouvimov, A.A. Nepapushev, A.S. Mukasyan, Influence of the high-energy ball milling on structure and reactivity of the Ni + Al powder mixture. J. Alloys Comp. 577 (2013) 600–605.
32. A.S. Rogachev, Mechanical activation of heterogeneous exothermic reactions in powder mixtures, Russ. Chem. Rev. 88 (2019) 875–900. doi 10.1070/RCR4884.
33. A. Fourmont, S. Le Gallet, O. Politano, C. Desgranges, F. Baras, Effects of planetary ball milling on AlCoCrFeNi high entropy alloys prepared by spark plasma sintering: Experiments and molecular dynamics study, J. Alloys Comp. 820 (2020) 153448. doi 10.1016/j.jallcom.2019.153448.
34. F. Baras, Q. Bizot, A. Fourmont, S. Le Gallet, O. Politano, Mechanical activation of metallic powders and reactivity of activated nanocomposites: a molecular dynamics approach. Applied Physics A (2021) 127:555. https://doi.org/10.1007/s00339-021-04700-9
35. S. Plimpton, Fast parallel algorithms for short-range molecular dynamics, J. Comput. Phys. 117 (1995) 1–19. doi 10.1006/jcph.1995.1039.
36. X.W. Zhou, R.A. Johnson, H.N.G. Wadley, Misfit-energy-increasing dislocations in vapor-deposited CoFe/NiFe multilayers, Phys. Rev. B 69 (2004) 144113. doi 10.1103/physrevb.69.144113.
37. A. Perron, S. Garruchet, O. Politano, G. Aral, V. Vignal, Oxidation of nanocrystalline aluminum by variable charge molecular dynamics, J. Phys. Chem. Solids 71 (2010) 119–124. doi 10.1016/j.jpcs.2009.09.008.

38. S. Odunuga, Y. Li, P. Krasnochtchekov, P. Bellon, R.S. Averback, Forced chemical mixing in alloys driven by plastic deformation, Phys. Rev. Lett. 95 (2005) 651–654. doi 10.1103/PhysRevLett.95.045901.

39. A. Stukowski, Visualization and analysis of atomistic simulation data with OVITO–the Open Visualization Tool, Modelling Simul. Mater. Sci. Eng. 18 (2009) 015012. doi 10.1088/0965-0393/18/1/015012.

40. J.H. Li, L.T. Kong, B.X. Liu, Proposed definition of microchemical in- homogeneity and application to characterize some selected miscible/immiscible binary metal systems, J. Phys. Chem. B 2004, 108, p 16071-16076, doi:10.1021/jp047897x.

41. A.C. Lund, C.A. Schuh, Driven Alloys in the Athermal Limit, Phys Rev Lett. 91 (2003) 189–4. doi:10.1103/PhysRevLett.91.235505.

42. A.E. Ermakov, V.V. Kondrat'ev, Yu.N. Gornostyrev, V.L. Gapontsev, Deformation-induced phase instability in nanocrystalline alloys, Phys. Met. Metallogr. 88 (1999) 211–218.

43. M.J. Zehetbauer, G. Steiner, E. Schafler, A. Korznikov, E. Korznikova, Deformation induced vacancies with severe plastic deformation: Measurements and modelling, Mater. Sci. Forum 503–504 (2006) 57–64. http://www.scientific.net.

44. M. Vaidya, G.M. Muralikrishna, B.S. Murty, High-entropy alloys by mechanical alloying: A review, J. Mater. Res. 34 (2019) 664-686. DOI: 10.1557/jmr/2019/37

45. M. Vaidya, A. Prasad, A. Parakh, B.S. Murty, Influence of sequence of elemental addition on phase evolution in nanocrystalline AlCoCrFrNi: Novel approach to alloy synthesis using mechanical alloying, Mater. Design 126 (2017) 37-46.